Journal of Biomolecular NMR, **23:** 115–125, 2002.
KLUWER/ESCOM

Cross correlation rates between Curie spin and dipole-dipole relaxation in paramagnetic proteins: The case of Cerium substituted Calbindin D_{9k}

Ivano Bertini[a,b,*], Gabriele Cavallaro[a,b], Marta Cosenza[a,b], Rainer Kümmerle[c], Claudio Luchinat[a,d], Mario Piccioli[a,b] & Luisa Poggi[a,b]

[a]*Magnetic Resonance Center, University of Florence, Via Luigi Sacconi 6, 50019 Sesto Fiorentino, Italy;* [b]*Department of Chemistry, University of Florence, Via Della Lastruccia 5, 50019 Sesto Fiorentino, Italy;* [c]*Bruker Italiana s.r.l., Via G. Pascoli 70/3, 20133 Milan, Italy;* [d]*Department of Agricultural Biotechnology, University of Florence, P.le delle Cascine 28, 50144 Florence, Italy*

Received 11 January 2002; Accepted 27 March 2002

Key words: Calbinding, Cerium protein, cross-correlation, Curie relaxation, paramagnetic NMR, paramagnetic proteins

Abstract

Cross correlation rates between Curie spin relaxation and H-N dipole-dipole coupling ($\Gamma^{CS,DD}_{HM,HN}$) have been determined for a calcium binding protein, Calbindin D_{9k}, in which one of the two calcium ions is substituted with cerium(III). $\Gamma^{CS,DD}_{HM,HN}$ values depend on both the metal-to-proton distances and the M-H-N angles and can be used as an additional constraint in order to refine the solution structure of paramagnetic metalloproteins. For this purpose, we have implemented a new module (CCR-DYANA) in a version of the program DYANA (PARAMAGNETIC-DYANA), which can be used together with other paramagnetism-based constraints such as pseudocontact shifts, residual dipolar couplings and hyperfine based Karplus relationships. This integrated structure calculation protocol has the advantage that different paramagnetic-based constraints are treated by the same algorithm in a way that the efficiency of each class of constraints can be analyzed and compared.

Abbreviations: CaCeCb, Cerium substituted Calbindin D_{9k}; CaLaCb, Lanthanum substituted Calbindin D_{9k}, CSA, chemical shift anisotropy; DD, dipole-dipole interaction; CS, Curie Spin; $\Gamma^{CS,DD}$, cross correlation between Curie spin and dipole-dipole relaxation; $\Gamma^{CSA,DD}$, cross correlation between chemical shift anisotropy and dipole-dipole relaxation; CCR, cross correlated relaxation rates; PCS, pseudocontact shift; RACT, relaxation allowed coherence transfer; RDC, residual dipolar coupling.

Introduction

Cross correlation effects arising from the interference of relaxation mechanisms due to the presence of unpaired electron spin density were first observed in paramagnetic molecules in 1993 (Bertini et al., 1993) as relaxation allowed coherence transfer peaks (RACT) (Wimperis and Bodenhausen, 1987, 1989) in COSY spectra. RACT cross peaks are due to cross correlation between homonuclear dipole-dipole couplings and Curie spin relaxation (Qin et al., 1993; Bertini et al., 1993, 1994). Cross correlation rates involving ^{1}H-^{15}N dipolar couplings and Curie spin relaxation were also measured (Boisbouvier et al., 1999).

Diamagnetic cross correlation effects have been largely investigated over the last years. Experiments to investigate these effects were developed using two main approaches. One is based on the separation of cross correlation effects on the (strong) multiplet components (J-resolved Γ experiments) (Pervushin et al., 1997; Reif et al., 1997; Riek et al., 1999; Salzmann et al., 1999; Boisbouvier et al., 1999; Pellecchia et al., 1999; Kloiber et al., 2001; Mandal et al., 2001). The

*To whom correspondence should be addressed. E-mail: bertini@cerm.unifi.it

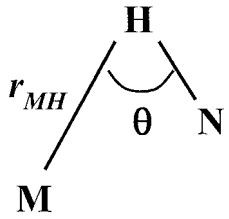

Scheme 1.

other is based on the selection of the (weak) signal arising from the relaxation-allowed coherence transfer (quantitative Γ experiments) (Goldman, 1984; Wimperis and Bodenhausen, 1987, 1989; Dalvit, 1992; Tjandra et al., 1996; Tessari et al., 1997; Yang et al., 1997, 1998; Felli et al., 1999; Chiarparin et al., 1999; Chiarparin et al., 2000; Tessari and Vuister, 2000).

Cross correlation rates between Curie spin relaxation (Guéron, 1975; Vega and Fiat, 1976) and H-N dipole-dipole coupling ($\Gamma^{CS,DD}_{HM,HN}$ hereafter) depend on the metal-to-proton distances and on the M-H-N angle as shown in Scheme 1. Therefore they constitute a type of constraint which is different with respect to other paramagnetism-based structural constraints (Bertini et al., 2001d). The potential role of this type of cross correlation as a constraint in structure calculation has been underlined several years ago (Bertini et al., 1994). Although several studies have been recently carried on from both experimental (Boisbouvier et al., 1999) and theoretical (Ghose and Prestegard, 1997; Desvaux and Gochin, 1999; Bertini et al., 2001a) points of view and although cross correlation rates have been used once for structural refinement (Hus et al., 2000), they have not yet been included within the most established protocols for structure calculation.

We present here the implementation of cross correlation rates as additional constraints within the program DYANA (Güntert et al., 1997).

To date, most of the available NMR structures of paramagnetic proteins have been solved using various versions of the above program (Banci et al., 1998b; Turner et al., 1998). Our version of DYANA, under the present collective name PARAMAGNETIC-DYANA (Barbieri et al., 2002), has been progressively implemented by us by the insertion of new modules permitting the use of pseudocontact shifts (PSEUDYANA) (Banci et al., 1998b), residual dipolar couplings (RDCDYANA-ORIENT) (Banci et al., 1998a), residual dipolar couplings derived angles (RDCDYANA-ANGLES) (Barbieri et al., 2002), or hyperfine derived dihedral angles (HYPERDYANA) (Banci et al., 2002) as structural constraints. The development of the cross correlation module in the same program has the obvious advantage that different paramagnetism-based constraints are treated by the same algorithm and in a way that the efficiency of each class of constraints can be analyzed and compared.

All sequences that measure diamagnetic $\Gamma^{CSA,DD}_{H,HN}$ can be used to measure $\Gamma^{CS,DD}_{HM,HN}$ in paramagnetic systems. Being $\Gamma^{CS,DD}_{HM,HN}$ a function of r^{-3}_{MH}, the build-up of this cross correlation competes with Curie self-relaxation. The detection of $\Gamma^{CS,DD}_{HM,HN}$ may be therefore not trivial. We discuss here two sequences (Tessari et al., 1997; Boisbouvier et al., 1999) based on the two main approaches discussed above. As a test case, we present the results of an NMR investigation performed over the di-calcium binding protein Calbindin D_{9k} selectively substituted with Ce^{3+} at the C-terminal site (CaCeCb hereafter) (Allegrozzi et al., 2000).

Calbindin D_{9k} is implicated in intracellular Ca^{2+} transport (Linse et al., 1987). Addition of Ln^{3+} salts to the holo-protein causes the selective replacement of Ca^{2+} in site II to obtain a CaLnCb derivative (Allegrozzi et al., 2000). No substantial differences in terms of structures (Bertini et al., 2001e) and dynamics (Bertini et al., 2002) were found between the native CaCaCb protein and the various CaLnCb derivatives nor among the various lanthanide substituted derivatives (Bertini et al., 2001c; Allegrozzi et al., 2000). The charge effect induced by the replacement of divalent calcium ion with trivalent metal ions affects only a few chemical shift values in the immediate proximity of the metal center, especially for the ^{15}N shifts (Biekofsky et al., 1998; Allegrozzi et al., 2000; Bertini et al., 2001d). Still, as extensively shown by NMR, no structural difference occurs besides the immediate proximity of the metal center (Bertini et al., 2001b). Therefore we focus here on the paramagnetic CaCeCb derivative (one unpaired electron), and we used the CaLaCb derivative as a safe diamagnetic analog of CaCeCb, as already extensively discussed (Bertini et al., 2001c, e, 2002).

Cross correlation rates were measured for the Ce^{3+} substituted derivative as well as for the analog diamagnetic derivative CaLaCb. The comparison with a diamagnetic analog has allowed us to separate, from the overall cross correlation rates due to ^1H chemical shift anisotropy (CSA), the contribution due to Curie spin relaxation.

Materials and methods

Sample preparation

The expression system was a generous gift of Prof. S. Forsén. Protein expression (Brodin et al., 1986) and purification (Johansson et al., 1990) of Bovine Pro43 → Met43 (P43M) mutant Calbindin D_{9k} were performed as reported (Malmendal et al., 1998; Chazin et al., 1989). Uniformly ^{15}N-labeled P43M was obtained from M9 minimal medium containing $^{15}NH_4Cl$ as the sole nitrogen source. NMR samples were prepared by dissolving the lyophilized protein in 550 μL of 10% D_2O/90% H_2O to finally obtain 2.0 mM protein solutions. The pH was adjusted to 6.0 by means of 0.1 M NaOH or 0.1 M HCl. Lanthanide-containing Calbindin D_{9k} samples were obtained by titrating the Ca^{2+} form of P43M with 0.1 M solutions of analytical grade $CeCl_3$ or $LaCl_3$. Titrations were followed by 1D ^{1}H NMR and by 2D ^{1}H-^{15}N HSQC spectroscopy. The samples were kept at 4 °C between measurements.

NMR spectroscopy

The experiments have been carried out at 300 K on a Bruker AVANCE spectrometer operating at 800 MHz ^{1}H resonance frequency. Quantitative measurements of cross-correlation rates between ^1H_N CSA and ^{1}H-^{15}N dipole-dipole relaxation were performed using a slightly modified version of a pulse sequence previously proposed (Tessari et al., 1997). The sequence is shown in supplementary material. In order to keep the water magnetization along the +z axis rather than the −z axis after the evolution of cross correlation, the phase of the first 90° proton pulse (ϕ1) has been changed from the originally proposed (−x −x x x) to (x x −x −x). For the same purpose in the reference experiment phase ϕ4 has been kept constant (−x) instead of (−x −x x x). This prevents radiation damping effects during t_1 and results in a significant reduction of the residual water signal that leads to an increased dynamic range. Possible radiation damping effects during the constant time period 4T are expected to equally affect both cross correlation and reference experiment, and therefore they should not give rise to systematic errors. Water signal suppression has been achieved by gradient coherence selection. Spectral widths were 11161 and 2432 Hz in the ^{1}H and ^{15}N dimensions, respectively. Acquisitions and recycle delays were 0.092 s and 1.3 s respectively. Spectra have been acquired using 128 repetitions with 2048 points in the f_2 dimension (^{1}H) and 200 points in the f_1 dimension (^{15}N). For a complete set of experiments two reference spectra were recorded and five cross correlation experiments were performed varying the cross correlation evolution period (Δ) from 4 ms to 20 ms. Raw data were processed with the Bruker XWINNMR software. A 90° shifted squared sine-bell apodization function was applied in both dimensions prior to Fourier transformation to obtain a final matrix of 2048 × 1024 real data points. A polynomial baseline correction has been performed in both dimensions.

For comparison purposes, experiments were also performed with the sequence proposed by Boisbouvier et al. (1999). The decay of each of the two components of the HN doublet was monitored by 6 experiments, at 2.9, 10, 15, 20, 25, 30 ms of decay time. All other parameters were the same as previously described.

Spectra analysis

Volume integration within the Bruker XWINNMR software was used for the analysis of the 2D spectra. For the reference experiments the mean value of two independent experiments has been calculated. The build-up curve of the ratios (cross-correlation/reference experiment) was fitted with a linear function (Tessari et al., 1997) using a least square method, according to Equation 1

$$\frac{I^{cc}}{I^{ref}} = -2\Gamma_{H,HN}\Delta\pi, \tag{1}$$

where Δ is the delay for the evolution of cross correlation, ranging from 4 ms to 20 ms, as described in supplementary material and (Tessari et al., 1997) and $\Gamma_{H,HN}$ is the observed cross correlation rate between ^{1}H CSA and ^{1}H-^{15}N dipole-dipole coupling.

Development of CCR-DYANA, the PARAMAGNETIC-DYANA module for cross correlation rates

In the case of isotropic molecular motions and isotropic magnetic susceptibility tensors, the cross correlation rate, expressed in Hertz, due to the interference of Curie spin relaxation and dipole-dipole ^{1}H-^{15}N coupling is given by (Bertini et al., 1993, 2001d; Ghose and Prestegard, 1997):

$$\Gamma^{CS,DD}_{HM,HN} = \frac{2}{15\pi}\left(\frac{\mu_0}{4\pi}\right)^2 \frac{B_\circ \gamma_H^2 \gamma_N \hbar g_J^2 \mu_B^2 J(J+1)}{(3kT) r_{NH}^3 r_{MH}^3} \left(4\tau_c + \frac{3\tau_c}{1+\omega_0^2\tau_c^2}\right)\left(3\cos^2\theta - 1\right), \tag{2}$$

where θ is the angle between the M-H and HN vectors, r_{MH} represents the distance between the amide proton and the electronic spin which is assumed to be localized on the metal, τ_c is the rotational correlation time of the molecule assumed rigid and all other symbols have their usual meanings. Note that, Equation 2 is the correct form of the cross correlation equation for lanthanide ions, where both electron spin S and g_e are replaced by the total angular momentum quantum number J and g_J.

The experimental value $\Gamma^{CS,DD}_{HM,HN}$ can be expressed as

$$\Gamma^{CS,DD}_{HM,HN} = \frac{K}{r^3_{MH}}\left(3\cos^2\theta - 1\right), \tag{3}$$

where the numerical constant K depends on the nucleus investigated, on the coupling involved, on the electron spin quantum number originating the Curie spin relaxation, and obviously on temperature, magnetic field and molecular tumbling.

The program DYANA calculates three-dimensional protein structures through molecular dynamics in torsion angle space (TAD), using a fast recursive algorithm to integrate the equations of motion (Güntert et al., 1997). The degrees of freedom are exclusively torsion angles, since the covalent structure parameters (bond lengths, bond angles, chiralities and planarities) are kept fixed at their optimal values during the calculation. The role of potential energy in TAD is carried out by the target function, which measures the violations of the experimental constraints in the calculated structure. A new pseudopotential term, U_{ccr}, has been added to PARAMAGNETIC-DYANA target function. When different data sets involving different paramagnetic metals are available, U_{ccr} has the following general form:

$$U_{ccr} = W\Sigma_m\Sigma_i w_{im}(\Gamma^{calc}_{im} - \Gamma^{obs}_{im})^2, \tag{4}$$

where Γ^{calc}_{im} is the ith calculated Γ value for the mth metal, Γ^{obs}_{im} and w_{im} are the corresponding observed value and the relative weight, respectively, and W is a global weighting factor. Any Γ^{calc}_{im} is expressed as in Equation 3, with K depending on the metal. K values are provided as an input by the user, together with the weighting factors and the observed Γ values.

In order to integrate the equations of motion in PARAMAGNETIC-DYANA, explicit expressions for the torques about the rotatable bonds, i.e., the gradients of the potential energy with respect to torsion angles, are required. The derivative of the pseudopotential U_{ccr} with respect to the kth torsion angle α_k has the following form:

$$\begin{aligned}\partial U_{ccr}/\partial\alpha_k = & 2W\Sigma_m K_m \Sigma_i w_{im}(\Gamma^{calc}_{im} - \Gamma^{obs}_{im}) \\ & [(a_i\mathbf{A_i} + b_i\mathbf{C_i})\cdot\mathbf{e_k} + (a_i\mathbf{B_i} + b_i\mathbf{D_i}) \\ & \cdot(\mathbf{e_k}\times\mathbf{r_{3k}})],\end{aligned} \tag{5}$$

where $\mathbf{e_k}$ is the unit vector directed along the kth rotatable bond, $\mathbf{r_{3k}}$ is the position vector of the third atom defining the kth torsion angle, and:

$$\begin{aligned} a &= [6\cos\theta r_{MH} r_{NH}^{-1} + 3(1 - 5\cos^2\theta)]/r^5_{MH}, \\ b &= -6\cos\theta/r^4_{MH} r_{NH}, \\ \mathbf{A} &= \mathbf{r}_M \times \mathbf{r}_H, \\ \mathbf{B} &= \mathbf{r}_M - \mathbf{r}_H, \\ \mathbf{C} &= \mathbf{r}_M \times \mathbf{r}_N, \\ \mathbf{D} &= \mathbf{r}_M - \mathbf{r}_N, \end{aligned} \tag{6}$$

$\mathbf{r}_M$, $\mathbf{r}_H$ and $\mathbf{r}_N$ being the position vectors of M, H and N atoms, respectively.

Several test calculations performed using a data set of simulated cross correlation values have shown that the choice of the weighting factors (w_{im}) is critical for a fruitful use of these constraints, since they dramatically influence the convergence of the calculations. The rationale for this behaviour is that a notable range of M-H distances is generally found in a single data set of observed Γ values, i.e., Γ values are available for residues near to the metal, as well as for residues far from the metal. As a consequence of the dependence of Γ on the reciprocal of the third power of M-H distance (see Equation 3), comparable deviations from the ideal conformation for N-H vectors with notably different distances from the metal center correspond to potential energies and torques of different orders of magnitude. Therefore, if similar weighting factors were used for all observed Γ's, structure annealing would be driven only by the constraints applied to residues with the shortest M-H distances. In all the calculations here performed, we have adopted a protocol which we believe to be general and applicable to any other systems, provided that a preliminary structure is available. In particular, we have chosen to set each w_{im} proportional to r^3_{MH}, obtained from the preliminary structure (Bertini et al., 2001e). In the present case, w values span from about 80 to about 9.8×10^3. The overall weighting factor W has been empirically set to 10^{-4} to properly scale U_{ccr} with respect to the other pseudopotentials. Such an empirical scaling is needed whenever constraints of different nature are used together in structure calculations (Bertini et al., 2001e; Banci et al., 1998b). The search of the scaling factor

is targeted at finding the smallest value which makes the single class of constraints effective in structure calculations when it is used together with the whole body of available constraints without an unreasonable increase of the target function for the other constraints. On the other hand, the value of W must be such that the precision of the resulting structure is not greater than the intrinsic precision of the experimental data. In the present case, the value of $W = 10^{-4}$ has been determined through test calculations performed using a set of simulated data.

Structure determination

Torsion Angle Dynamics (TAD) combined with a simulated annealing algorithm was performed with the newly implemented PARAMAGNETIC-DYANA to calculate families of 200 structures starting from randomly generated conformers in 10 000 annealing steps. The program PROCHECK was used to analyze the calculated structures (Laskowski et al., 1996).

Results and discussion

Measurement of cross correlation rates between Curie spin and dipole-dipole H-N relaxation

In the case of a paramagnetic molecule, experiments designed to observe cross correlation rates (CCR hereafter) between ^{1}H CSA and dipole-dipole ^{1}H-^{15}N coupling (Tessari et al., 1997; Boisbouvier et al., 1999), measure the sum of the CSA arising from diamagnetic ^{1}H CSA and the component of ^{1}H CSA induced by Curie spin relaxation. The latter is quantified by Equation 2. The electronic properties of lanthanide ions are peculiar. Spin orbit interactions are larger than ligand field effects and therefore, both the quantum number J and the g_J factor replace the electron spin number S and g_e in all equations describing the paramagnetic relaxation. In the case of Ce^{3+}, $J = 5/2$ and $g_J = 6/7$. To separate these effects, the CaLaCb derivative, a diamagnetic analog of CaCeCb, has also been studied. CaLaCb has been preferred to the native Ca_2Cb derivative because of the conservation of the metal ion charge (Bertini et al., 2001e). Neglecting the occurrence of possible differences between the 'diamagnetic' ^{1}H CSA operative in CaLaCb and CaCeCb, the contribution to cross correlation rates arising from the presence of the unpaired electron spin is given by

$$\Gamma^{CS,DD}_{HM,HN} = \Gamma^{CSA,DD}_{H,HN}\text{CaCeCb} - \Gamma^{CSA,DD}_{H,HN}\text{CaLaCb}. \quad (7)$$

Cross correlation rates between ^1H_N CSA and ^{1}H-^{15}N dipole relaxation were recorded, at 800 MHz, according to the approach proposed by Tessari et al. (1997), on both CaLaCb and CaCeCb as well as with the TROSY-based pulse sequence proposed by Boisbouvier et al. (1999). While the former sequence selects the signal arising from a Relaxation Allowed Coherence Transfer (RACT hereafter) pathway (Bertini et al., 1994) and a reference experiment is needed to account for auto-relaxation effects, the latter selects the two multiplet components through a TROSY (Pervushin et al., 1997) sequence and then measures T_2 relaxation rates through a spin echo block, in order to extract the differential relaxation rate. In principle, we expect the TROSY based pulse sequence to be more suitable for the study of fast relaxing signals, because the timing of the sequence, which has been specifically designed to work with paramagnetic molecules, is much shorter with respect to a sequence in which a constant time period is needed to build up the RACT signal and to account for auto relaxation.

However, in the presently investigated system, none of the peaks observed in the TROSY based approach was lost in the RACT based experiment. The sequence by Tessari et al. (1997) (reported in supplementary material for the reader's convenience) gave experimental data which, on average, provided a satisfactory linear fit as shown in Figure 1. In the case of the J-resolved Γ experiment (Boisbouvier et al., 1999), the scattering of the data with respect to their expected exponential decay made the analysis less reliable.

The $\Gamma^{CS,DD}_{HM,HN}$ value obtained using the RACT based experiment range from -15.9 to 3.1 hz. For ten HN signals (residues 23, 24, 53, 54, 61, 63, 64, 65, 66, 68), $\Gamma^{CS,DD}_{HM,HN}$ is large and is measured with a small relative error. For the remaining 42 residues, observed rates are small and their absolute values are of the same magnitude or even smaller than the experimental errors. Nevertheless, all of these values have been included in CCR-DYANA, because even small values represent a meaningful structural constraint in terms of metal-to-proton distance and/or HN vector orientation. The error has been taken into consideration as a specific tolerance (see later).

Of course, $\Gamma^{CS,DD}_{HM,HN}$ is also affected by internal mobility. Such a contribution can be taken into account by monitoring internal motions through the measurement of $\Gamma^{CSA,DD}_{N,HN}$ in the CaLaCb derivative (Bertini

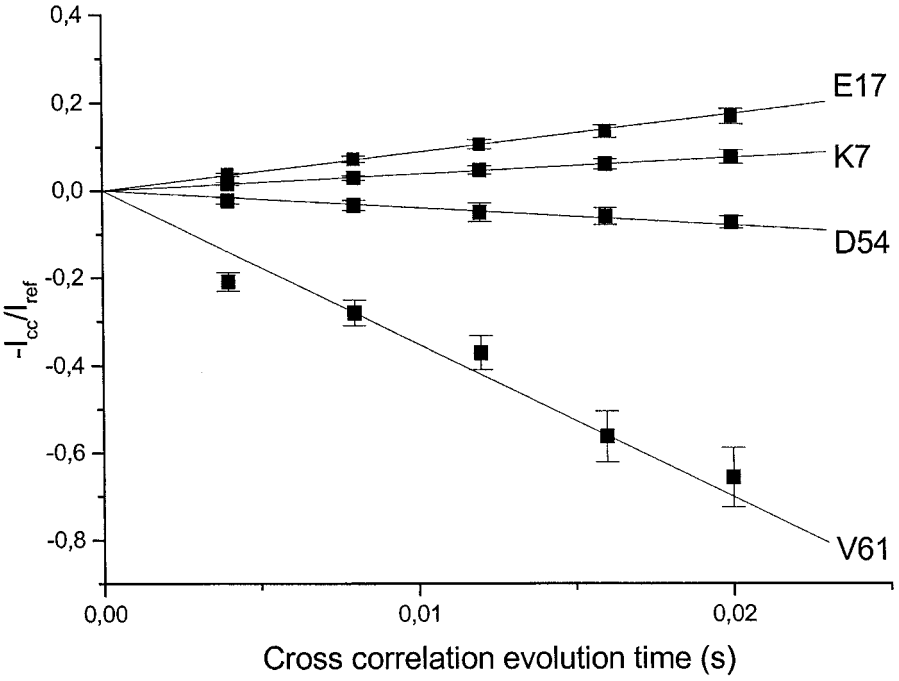

Figure 1. Representative build-up curves of $-I_{cc}/I_{ref}$ for selected residues. The intensity ratio between the relaxation allowed coherence transfer experiments (I_{cc}) and the reference INEPT transfer experiment (I_{ref}) is reported as a function of the cross correlation evolution time (4Δ, see supplementary material). Experiments have been recorded at 800 MHz, 300 K. The V61 data refer to the NH group closest to the metal that gives rise to observable an HSQC peak. Its slope is the largest observed.

et al., 2002). These measurements, which confirm the results previously obtained from model free analysis of several Calbindin D_{9k} mutants (Akke et al., 1991, 1993; Kordel et al., 1993), show that the region spanning residues 42–45 undergoes internal mobility. For these residues, $\Gamma^{CSA,DD}_{N,HN}$ values were found in the range 4.7–6.9 s^{-1}. They are substantially lower than the average values observed in this protein which is 9.2 ± 0.7 s^{-1}. The same considerations hold for the C-terminal residue 75. In principle, Equation 2 could be multiplied by an order parameter S^2. However, for most residues S^2 is ≅ 0.9 and the correction would be well within the experimental error, while for the residues experiencing substantial mobility it is well known that correcting by S^2 may be a dangerous approximation (de Alba et al., 1999). Therefore $\Gamma^{CS,DD}_{HM,HN}$ values of these residues were excluded from calculations, and only 47 out of 52 experimental values have been used for structure calculations (Table 1).

Refinement using CCR-DYANA

Forty-seven CCR were used as input for CCR-DYANA where the numeric constant K in Equation 3 was given a value of −1360 Hz Å^3. This value is critical for the use of CCR as structural constraints. In the present case a τ_r value of 4.3 ns could be estimated from the ModelFree analysis (Akke et al., 1993). The use of such CCR values over a structure calculated with more than 1700 NOEs provides a decrease in the RMSD of about 10%, accomplished with a small increase of the overall target function. Given the small amount of additional constraints (about 3% of the overall number of constraints) the obtained results, which are shown in Table 2, indicate that CCR are quite effective on the refinement of the family of structures. This is also accompanied by a small improvement of the Ramachandran plot statistics. As expected, the number and magnitude of deviations between experimental CCR values and those calculated from the various families are smaller in the structures obtained using the above data as constraints. This is evident in Figure 2, which shows a comparison of calculated and experimental CCR values before (A) and after (B) refinement. As observed in Table 2, experimental CCR would give a contribution to the Target Function of about 1.5 Å^2 when calculated on the NOE only structure. The inclusion of CCR constraints de-

Table 1. Cross correlation rates (Hz) measured at 800 MHz

AA	CaCeCb Γ^a	CaLaCb Γ^a	(Ce-La) Γ^a
1	0.9 +/− 0.3	1.1 +/− 0.3	−0.2 +/− 0.4
2	1.6 +/− 0.3	1.8 +/− 0.3	−0.2 +/− 0.4
4	1.1 +/− 0.2	1.1 +/− 0.2	−0.1 +/− 0.3
5	2.0 +/− 0.4	1.7 +/− 0.4	0.3 +/− 0.6
6	1.8 +/− 0.4	1.6 +/− 0.3	0.1 +/− 0.5
7	1.4 +/− 0.3	1.7 +/− 0.3	−0.2 +/− 0.4
8	2.2 +/− 0.1	2.5 +/− 0.3	−0.3 +/− 0.3
9	1.4 +/− 0.3	1.4 +/− 0.3	−0.1 +/− 0.4
10	1.9 +/− 0.4	1.6 +/− 0.3	0.3 +/− 0.5
11	1.7 +/− 0.3	1.8 +/− 0.2	0.0 +/− 0.3
12	2.0 +/− 0.4	1.5 +/− 0.3	0.6 +/− 0.5
15	1.6 +/− 0.2	1.3 +/− 0.3	0.3 +/− 0.3
16	1.6 +/− 0.3	1.2 +/− 0.2	0.4 +/− 0.4
17	3.2 +/− 0.3	2.7 +/− 0.3	0.5 +/− 0.5
18	2.9 +/− 1.0	3.1 +/− 1.1	−0.2 +/− 1.5
19	1.9 +/− 0.6	2.1 +/− 0.6	−0.2 +/− 0.8
21	2.8 +/− 0.1	2.3 +/− 0.2	0.5 +/− 0.3
22	1.8 +/− 0.3	1.5 +/− 0.2	0.3 +/− 0.3
23	1.6 +/− 0.2	2.8 +/− 0.6	−1.2 +/− 0.6
24	1.2 +/− 0.1	2.8 +/− 0.2	−1.6 +/− 0.3
27	1.9 +/− 0.3	1.7 +/− 0.3	0.2 +/− 0.4
28	2.0 +/− 0.4	1.9 +/− 0.4	0.0 +/− 0.6
31	1.2 +/− 0.1	1.6 +/− 0.1	−0.4 +/− 0.1
33	2.0 +/− 0.3	2.1 +/− 0.2	−0.2 +/− 0.4
34	1.3 +/− 0.2	1.6 +/− 0.2	−0.3 +/− 0.2
35	1.7 +/− 0.2	2.0 +/− 0.2	−0.3 +/− 0.3
36	2.5 +/− 0.4	2.2 +/− 0.4	0.3 +/− 0.6
38	1.9 +/− 0.7	1.7 +/− 0.6	0.2 +/− 0.9
39	1.9 +/− 0.4	1.5 +/− 0.3	0.4 +/− 0.5
40	1.5 +/− 0.2	1.7 +/− 0.3	−0.2 +/− 0.4
41	0.9 +/− 0.2	0.9 +/− 0.2	0.0 +/− 0.3
46	2.6 +/− 0.6	2.2 +/− 0.6	0.4 +/− 0.8
48	1.2 +/− 0.1	1.6 +/− 0.3	−0.4 +/− 0.3
49	1.6 +/− 0.4	1.5 +/− 0.2	0.2 +/− 0.5
52	1.5 +/− 0.3	1.5 +/− 0.2	0.0 +/− 0.4
53	2.8 +/− 0.6	1.6 +/− 0.3	1.2 +/− 0.7
54	−1.4 +/− 0.1	1.9 +/− 0.4	−3.3 +/− 0.4
61	−12.6 +/− 1.3	3.3 +/− 0.2	−15.9 +/− 1.3
63	6.1 +/− 0.5	3.0 +/− 0.2	3.1 +/− 0.5
64	2.6 +/− 0.2	1.0 +/− 0.2	1.6 +/− 0.3
65	2.9 +/− 0.4	1.6 +/− 0.3	1.3 +/− 0.5
66	2.6 +/− 0.3	1.4 +/− 0.6	1.2 +/− 0.7
68	−0.8 +/− 0.1	1.2 +/− 0.2	−2.0 +/− 0.3
69	1.5 +/− 0.3	1.8 +/− 0.4	−0.4 +/− 0.5
71	1.0 +/− 0.2	1.4 +/− 0.2	−0.4 +/− 0.3
72	1.1 +/− 0.2	1.3 +/− 0.2	−0.2 +/− 0.3
74	1.0 +/− 0.3	1.1 +/− 0.3	−0.1 +/− 0.4

[a] $\Gamma = 2\eta/\pi$.

creases their contribution from 1.50 Å^2 to 0.11 Å^2, while the increase of the other constraints is only from 0.10 Å^2 to 0.74 Å^2 without consistent violation. This suggests (Bax et al., 2001; Tjandra et al., 2000; Clore and Garrett, 1999; Banci et al., 1998a) that the accuracy of the structure is actually improved by the introduction of the CCR constraints, which are shown to be consistent with the others.

To compare the effects induced by the insertion of CCR with the effect provided by the introduction of pseudocontact shifts (PCS) and of residual dipolar couplings (RDC), we performed analogous calculations using NOEs only plus RDC or PCS (Table 2). The addition of 64 RDC produces a very small decrease in RMSD, while the addition of 135 pseudocontact shifts arising from backbone assignment of NH groups provides almost the same effects as CCR in terms of RMSD decrease. All the different types of paramagnetic constraints provide an improvement of the Ramachandran plot. The improvement is larger in the case of RDC and less pronounced for CCR and PCS.

Overall, CCR have a sort of intermediate behavior in comparison with PCS and RDC. Indeed, CCR are almost independent on any external tensor and they act as three center (M-H-N) distance constraints. Therefore we expect them to be more efficient in terms of RMSD decrease and relatively inefficient in terms of improvement of Ramachandran plot. They are complementary with respect to RDC (Bertini et al., 2001g). Starting from the NOE only based structure, we may expect two different types of refinement arising from these two classes of constraints, RDC and CCR. While RDC provide a backbone rearrangement which improves the statistics of the Ramachandran plot, CCR provide an increase in the precision of the calculated structures which essentially involves those regions of the protein which are relatively disordered because of the quenching of the NOE information due to the presence of the unpaired electron spin (Bertini et al., 2001e). In the present case, an improvement is observed in the region 50–66, with a substantial improvement on residues 54–62, that encompasses the loop II (Ce^{3+} binding site). This is shown in Figure 3. For both RDC and CCR the constraints act as a stress imposed to the NOE only structures and result in an increase of the target function which is however fully acceptable (Table 2).

PCS have a nucleus-to-metal distance dependent component and an orientation dependent component, where the orientation is defined with respect to the

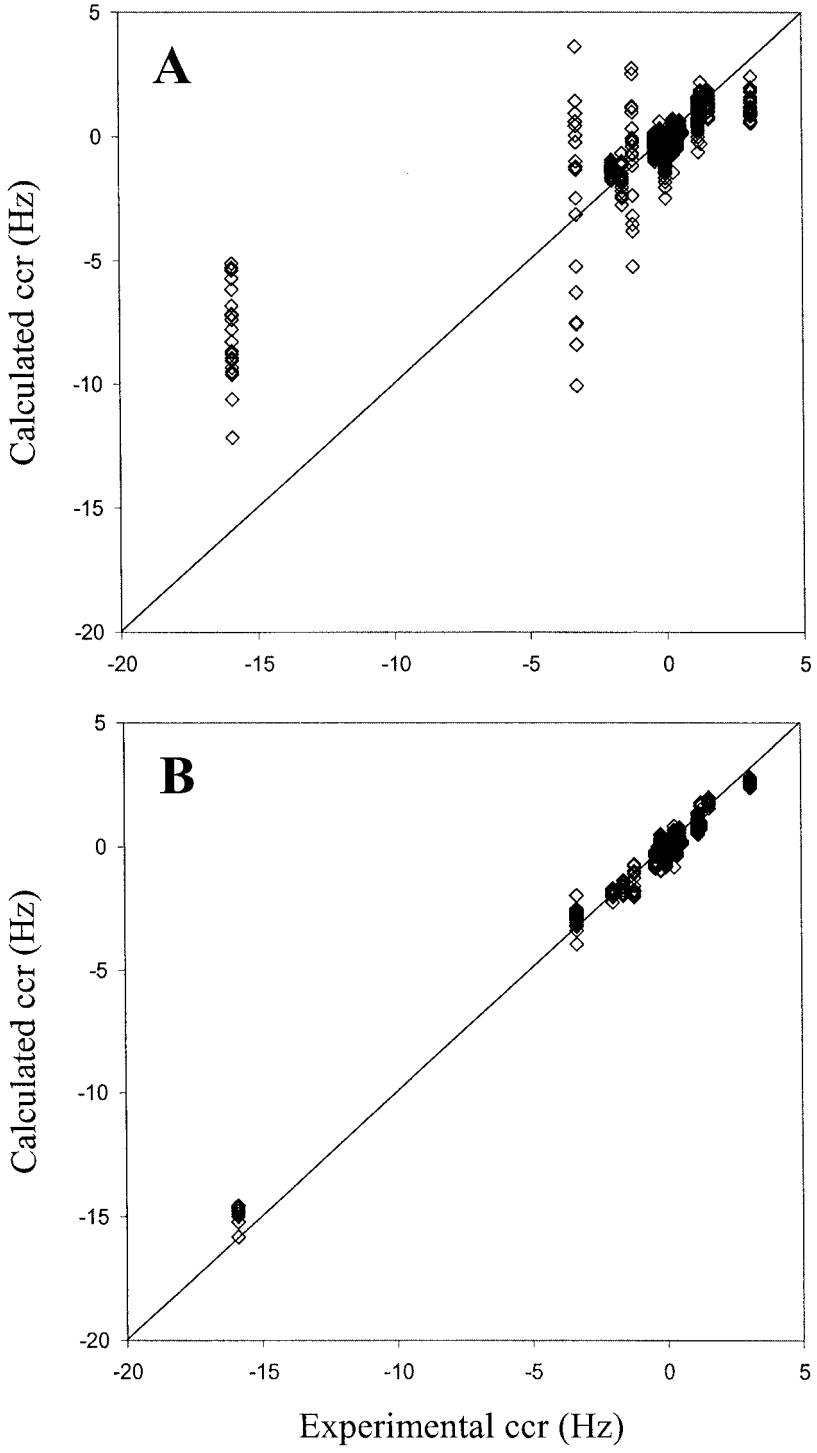

Figure 2. Comparison of observed versus calculated cross correlation rates before (A) and after (B) structure refinement with the CCR constraints. Data relative to all twenty conformers of the family are shown. The diagonal is also shown.

Table 2. The effect of the various type of constraints into structure calculation

Restraints used	Global			Ramachandran			
	bb RMSD pw (2–75)	TF Total	TF CCR	Core (%)	All. (%)	Gen. (%)	Not All. (%)
NOEs only	1.00 ± 0.17	0.10 ± 0.01	(1.50 ± 0.33)[a]	69.2	27.7	1.5	1.5
NOEs and CCR	0.89 ± 0.17	0.74 ± 0.07	0.11 ± 0.07	76.9	21.5	1.5	0
NOEs and PCS	0.86 ± 0.14	0.14 ± 0.01	(1.52 ± 0.39)[a]	72.3	26.2	0	1.5
NOEs and RDC	0.96 ± 0.17	0.36 ± 0.03	(1.71 ± 0.42)[a]	80.0	16.9	3.1	0
NOEs, CCR and PCS	0.82 ± 0.15	0.88 ± 0.09	0.14 ± 0.09	76.9	21.5	1.5	0
NOEs, CCR and RDC	0.90 ± 0.17	1.18 ± 0.07	0.14 ± 0.07	73.8	21.5	4.6	0
NOEs, CCR, PCS and RDC	0.76 ± 0.11	1.44 ± 0.08	0.16 ± 0.08	80.0	16.9	3.1	0

[a]Values in parenthesis show the violations of the CCR values when they are not included as constraints in the structure refinement.

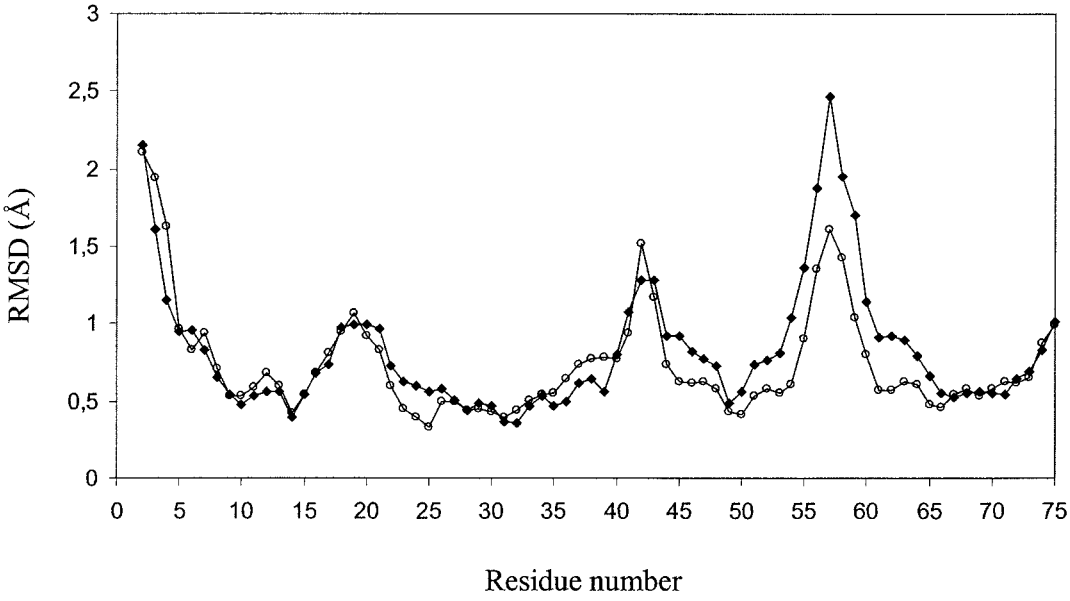

Figure 3. RMSD values per residue before (filled diamonds) and after (empty circles) structure refinement with the CCR constraints.

magnetic anisotropy tensor originated by the electron spin. In turn, the magnetic anisotropy components as well as the orientation of the tensor were recalculated as the refinement of the structure improves, until convergence. The recalculated tensor after each refinement step was obtained using the program FANTASIA (Banci et al., 1997). This allows the distance dependent part of PCS to be as effective in terms of RMSD refinement as for CCR, but, at variance with them, the contribution to the target function is much smaller because the magnetic susceptibility tensor is also calculated with this same procedure.

The number of PCS that can be obtained is more than double with respect to RDC and CCR. This is obviously expected because both ^{1}H and ^{15}N PCS are directly available by simple comparison of HSQC experiments, while additional experiments must be collected to measure RDC and CCR, thus resulting in the loss of information for some of the peaks.

It should also be noted that a relatively large tolerance must be applied to CCR experimental data in order to properly account for experimental error. Indeed, experimental errors in CCR measurements must take into account that cross correlation rates arising form the Curie spin relaxation and the HN dipole-dipole coupling are obtained as a relatively small difference between two large values independently measured on the CaCe derivative and on an analog diamagnetic system.

This relatively large tolerance accounts also for the fact that CCR constraints are added as structural constraints under the hypothesis of isotropic magnetic susceptibility tensor. Indeed, effects of anisotropic magnetic susceptibility on CCR are theoretically expected (Bertini et al., 2001a). Although in principle these effects are not negligible, they are expected to be smaller, or of the same order of magnitude, of the tolerance that have been given to the experimental data.

Finally, a comment is due on the choice of setting the weighting factors w_{im} (see Equations 4 and 5) proportional to r_{MH}^3. As $\Gamma_{\mathrm{im}}^{\mathrm{calc}}$ depends on the reciprocal of the third power of the distance between the proton and the paramagnetic center (Equations 2 and 3), a small motion (e.g., an angular variation) of a NH vector near the metal ion sizeably alters its $\Gamma_{\mathrm{im}}^{\mathrm{calc}}$ value, while the same motion for a NH vector far from the metal ion produces a much smaller change of the $\Gamma_{\mathrm{im}}^{\mathrm{calc}}$ value. In order to avoid that vectors close to the paramagnetic center drive the whole simulated annealing process, at the cost of the good convergence of the calculation, M-H distance must be taken into account in the evaluation of the $\partial U_{\mathrm{ccr}}/\partial \alpha_{\mathrm{k}}$ (Equation 5) contribution to the total gradient of the target function. The choice of setting the weighting factors w_{im} proportional to r_{MH}^3, is based on the functional form of $\Gamma_{\mathrm{im}}^{\mathrm{calc}}$ itself. This allows to resize the torques acting on NH vectors at different distances from the metal center to the same order of magnitude.

One could think of directly implementing into the source code of the program a protocol that allows the re-scaling of the w_{im}'s during the calculation according to the metal-proton distance. However, if the starting structure is reliable, the estimate of the w_{im}'s is consequently good. Of course, they can be back-calculated on the resulting structure and used for a further refinement step, in an iterative fashion. In the present case, no improvement was observed in the second step, thus providing a check of the quality of the initial values for the w_{im}'s.

Conclusions

In summary, we have shown that cross correlation rates between Curie spin relaxation and dipole-dipole relaxation can be successfully exploited within classical structure calculation through an additional module of the program DYANA. As expected on the basis of their functional form, cross correlation rates affect the overall RMSD of the family of structures in a way that is similar to the effect due to PCS. The occurrence in the PCS functional form, of a dependence on the magnetic susceptibility tensor that is calculated together with the structure within a self consistent approach allows PCS to refine the structure with lower contribution to the target function with respect to CCR. On the other hand, the property of CCR of being scarcely sensitive to magnetic susceptibility anisotropy is a helpful feature of CCR constraints. The latter can, in principle, be exploited under more critical conditions than PCS. Indeed, when only a relatively small number of hyperfine shifted signals can be observed, the estimate of the magnetic susceptibility tensor may be difficult and therefore even PCS data are less efficiently exploited. In such cases, CCR may still be a valuable tool to obtain geometrical and structural information especially in those protein regions that are in close proximity to the paramagnetic center. Like PCS, the sphere of action of CCR can be tuned by the use of other, more paramagnetic, lanthanide ions such as Yb^{3+} and Dy^{3+}, for which measurable CCR effects can be found at larger distances from the metal, the closer protons being broadened beyond detection by Curie relaxation itself (Banci et al., 1991). Note that, although this is the same approach proposed (Bertini et al., 2001c) (Biekofsky et al., 1999) (Contreras et al., 1999) and successfully exploited (Bertini et al., 2001c) for RDC, the choice of the best lanthanide is not dictated by the magnetic anisotropy tensor but only by the quantum number J and by the g_J constant, which in the case of Ln^{3+} ions replace S and g_e in Equation 2 (Bertini et al., 2001f). Thus, we propose to use the CCR of various paramagnetic lanthanides to refine shells at variable distances from the metal ion.

Acknowledgements

This work was supported by the European Union Research and Training Network (RTN) Project 'Cross correlation between the fluctuations of different interactions: a new avenue for biomolecular NMR' (Contract No. HPRN-CT-2000-00092). The work has been performed at the EU Large Scale Facility PARABIO (Contract No. HPRI-CT-1999-00009). We acknowledge Dr Y.-M. Lee for providing us with Calbindin D_{9k} samples as well as Dr Wolfgang Bermel for stimulating discussions. GC is a fellow of the International Doctorate in Structural Biology, managed by

the Magnetic Resonance Center of the University of Florence.

References

Akke, M., Forsén, S. and Chazin, W.J. (1991) *J. Mol. Biol.*, **220**, 173–189.

Akke, M., Skelton, N.J., Kördel, J., Palmer, III, A.G. and Chazin, W.J. (1993) *Biochemistry*, **32**, 9832–9844.

Allegrozzi, M., Bertini, I., Janik, M.B.L., Lee, Y.-M., Liu, G. and Luchinat, C. (2000) *J. Am. Chem. Soc.*, **122**, 4154–4161.

Banci, L., Bertini, I., Cavallaro, G. and Luchinat, C. (2002) *JBIC*, **7**, 416–426.

Banci, L., Bertini, I., Gray, H.B., Luchinat, C., Reddig, T., Rosato, A. and Turano, P. (1997) *Biochemistry*, **36**, 9867–9877.

Banci, L., Bertini, I., Huber, J.G., Luchinat, C. and Rosato, A. (1998a) *J. Am. Chem. Soc.*, **120**, 12903–12909.

Banci, L., Bertini, I., Cremonini, M.A., Gori Savellini, G., Luchinat, C., Wüthrich, K. and Güntert, P. (1998b) *J. Biomol. NMR*, **12**, 553–557.

Banci, L., Bertini, I. and Luchinat, C. (1991) *Nuclear and Electron Relaxation. The Magnetic Nucleus-Unpaired Electron Coupling in Solution*, VCH, Weinheim.

Barbieri, R., Bertini, I., Cavallaro, G., Lee, Y.-M., Luchinat, C. and Rosato, A. (2002) *J. Am. Chem. Soc.*, **124**, 5581–5587.

Bax, A., Kontaxis, G. and Tjandra, N. (2001) *Meth. Enzymol.*, **339**, 127–174.

Bertini, I., Carrano, C.J., Luchinat, C., Piccioli, M. and Poggi, L. (2002) *Biochemistry*, **41**, 5104–5111.

Bertini, I., Kowalewski, J., Luchinat, C. and Parigi, G. (2001a) *J. Magn. Reson.*, **152**, 103–108.

Bertini, I., Lee, Y.-M., Luchinat, C., Piccioli, M. and Poggi, L. (2001b) *Chem. Bio Chem.*, **2**, 550–558.

Bertini, I., Janik, M.B.L., Lee, Y.-M., Luchinat, C. and Rosato, A. (2001c) *J. Am. Chem. Soc.*, **123**, 4181–4188.

Bertini, I., Luchinat, C. and Piccioli, M. (2001d) *Meth. Enzymol.*, **339**, 314–340.

Bertini, I., Donaire, A., Jimenez, B., Luchinat, C., Parigi, G., Piccioli, M. and Poggi, L. (2001e) *J. Biomol. NMR*, **21**, 85–98.

Bertini, I., Luchinat, C. and Parigi, G. (2001f) *Solution NMR of Paramagnetic Molecules*, Elsevier, Amsterdam.

Bertini, I., Janik, M.B.L., Liu, G., Luchinat, C. and Rosato, A. (2001g) *J. Magn. Reson.*, **148**, 23–30.

Bertini, I., Luchinat, C., Piccioli, M. and Tarchi, D. (1994) *Concepts Magn. Reson.*, **6**, 307–335.

Bertini, I., Luchinat, C. and Tarchi, D. (1993) *Chem. Phys. Lett.*, **203**, 445–449.

Biekofsky, R.R., Martin, S.R., Browne, J.P., Bayley, P.M. and Feeney, J. (1998) *Biochemistry*, **37**, 7617–7629.

Biekofsky, R.R., Huskett, F.W., Schmidt, J.M., Martin, S.R., Browne, J.P., Bayley, P.M., Feeney, J. (1999) *FEBS Lett.*, **460**, 519–526.

Boisbouvier, J., Gans, P., Blackledge, M., Brutscher, B. and Marion, D. (1999) *J. Am. Chem. Soc.*, **121**, 7700–7701.

Brodin, P., Grundstrom, T., Hofmann, T., Drakenberg, T., Thulin, E. and Forsén, S. (1986) *Biochemistry*, **25**, 5371–5377.

Chazin, W.J., Kördel, J., Drakenberg, T., Thulin, E., Brodin, P., Grundstrom, T. and Forsén, S. (1989) *Proc. Natl. Acad. Sci. USA*, **86**, 2195–2198.

Chiarparin, E., Pelupessy P., Ghose, R. and Bodenhausen, G. (1999) *J. Am. Chem. Soc.*, **121**, 6876–6883.

Chiarparin, E., Pelupessy P., Ghose, R. and Bodenhausen, G. (2000) *J. Am. Chem. Soc.*, **122**, 1758–1761.

Clore, G.M. and Garrett, D.S. (1999) *J. Am. Chem. Soc.*, **121**, 9008–9012.

Contreras, M.A., Ubach, J., Millet, O., Rizo, J. and Pons, M. (1999) *J. Am. Chem. Soc.*, **121**, 8947–8948.

Dalvit, C. (1992) *J. Magn. Reson.*, **97**, 645–650.

de Alba, E., Baber, J.L. and Tjandra, N. (1999) *J. Am. Chem. Soc.*, **121**, 4282–4283.

Desvaux, H. and Gochin, M. (1999) *Mol. Phys.*, **96**, 1317–1333.

Felli, I.C., Richter, C., Griesinger, C. and Schwalbe, H. (1999) *J. Am. Chem. Soc.*, **121**, 1956–1957.

Ghose, R. and Prestegard, J.H. (1997) *J. Magn. Reson.*, **128**, 138–143.

Goldman, M. (1984) *J. Magn. Reson.*, **60**, 437–452.

Guéron, M. (1975) *J. Magn. Reson.*, **19**, 58–66.

Güntert, P., Mumenthaler, C. and Wüthrich, K. (1997) *J. Mol. Biol.*, **273**, 283–298.

Hus, J.C., Marion, D. and Blackledge, M. (2000) *J. Mol. Biol.*, **298**, 927–936.

Johansson, C., Brodin, P., Grundstrom, T., Thulin, E., Forsén, S. and Drakenberg, T. (1990) *Eur. J. Biochem.*, **187**, 455–460.

Kloiber, K., Schuler, W. and Konrat, R. (2001) *J Biomol NMR*, **19**, 347–354.

Kordel, J., Skelton, N.J. and Chazin, W.J. (1993) *J. Mol. Biol.*, **231**, 711–734.

Laskowski, R.A., Rullmann, J.A.C., MacArthur, M.W., Kaptein, R. and Thornton, J.M. (1996) *J. Biomol. NMR*, **8**, 477–486.

Linse, S., Brodin, P., Drakenberg, T., Thulin, E., Sellers, P., Elmden, K., Grundstrom, T. and Forsén, S. (1987) *Biochemistry*, **26**, 6723–6735.

Malmendal, A., Carlström, G., Hambraeus, C., Drakenberg, T., Forsén, S. and Akke, M. (1998) *Biochemistry*, **37**, 2586–2595.

Mandal, P.K., Grandori, R., Hohenthanner, K. and Muller, N. (2001) *J. Biomol. NMR*, **20**, 31–37.

Pellecchia M., Pang Y., Wang, L., Kurochkin A.V., Kumar A. and Zuiderweg, E.R.P. (1999) *J. Am. Chem. Soc.*, **121**, 9165–9170.

Pervushin, K., Riek, R., Wider, G. and Wüthrich, K. (1997) *Proc. Natl. Acad. Sci. USA*, **94**, 12366–12371.

Qin, J., Delaglio, F., La Mar, G.N. and Bax, A. (1993) *J. Magn. Reson.*, **B102**, 332–336.

Reif, B., Hennig, M. and Griesinger, C. (1997) *Science*, **276**, 1230–1233.

Riek, R., Wider, G., Pervushin, K. and Wuthrich, K. (1999) *Proc. Natl. Acad. Sci. USA*, **96**, 4918–4923.

Salzmann, M., Wider, G., Pervushin, K., Senn, H. and Wüthrich, K. (1999) *J. Am. Chem. Soc.*, **121**, 844–848.

Tessari, M. and Vuister, G.W. (2000) *J. Biomol. NMR*, **16**, 171–174.

Tessari, M., Vis, H., Boelens, R., Kaptein, R. and Vuister, G.W. (1997) *J. Am. Chem. Soc.*, **119**, 8985–8990.

Tjandra, N., Marquardt, J. and Clore, G.M. (2000) *J. Magn. Reson.*, **142**, 393–396.

Tjandra, N., Szabo, A. and Bax, A. (1996) *J. Am. Chem. Soc.*, **118**, 6886–6891.

Turner, D.L., Brennan, L., Chamberlin, S.G., Louro, R.O. and Xavier, A.V. (1998) *Eur. Biophys. J.*, **27**, 367–375.

Vega, A.J. and Fiat, D. (1976) *Mol. Phys.*, **31**, 347–355.

Wimperis, S. and Bodenhausen, G. (1987) *Chem. Phys. Lett.*, **140**, 41–45.

Wimperis, S. and Bodenhausen, G. (1989) *Mol. Phys.*, **66**, 897–919.

Yang, D.W., Gardner, K.H. and Kay, L.E. (1998) *J. Biomol. NMR*, **11**, 213–220.

Yang, D.W., Konrat, R. and Kay, L.E. (1997) *J. Am. Chem. Soc.*, **119**, 11938–11940.